ACS Catalysis

Research Article

pubs.acs.org/acscatalysis

Alloying Pt Sub-nano-clusters with Boron: Sintering Preventative and Coke Antagonist?

Jonny Dadras,[†] Elisa Jimenez-Izal,[†] and Anastassia N. Alexandrova*[,†,‡]

[†]Department of Chemistry and Biochemistry, University of California, Los Angeles, California 90095, United States

[‡]California Nano-Systems Institute, Los Angeles, California 90095, United States

Supporting Information

ABSTRACT: Immobilized Pt clusters are interesting catalysts for dehydrogenation of alkanes. However, surface-deposited Pt clusters deactivate rapidly via sintering and coke deposition. The results reported here suggest that adding boron to oxide-supported Pt clusters could be a "magic bullet" against both means of deactivation. The model systems studied herein are pure and B-doped Pt clusters deposited on MgO(100). The nonstoichiometric boride cluster obtained via such alloying is found to anchor to the support via a covalent B−O bond, and the cluster-surface binding is much stronger than in the case of pure Pt clusters. Additionally, B introduces covalency to the intracluster bonding, leading to structural distortion and stabilization. The energy required to dissociate a Pt atom from a boride cluster is significantly larger than that of pure Pt clusters. These energetic arguments lead to the proposal that sintering via both Ostwald ripening and particle coalescence would be discouraged relative to pure Pt clusters. Finally, it is shown that the affinity to C also drops dramatically for borated clusters, discouraging coking and increasing the selectivity of potential cluster catalysts.

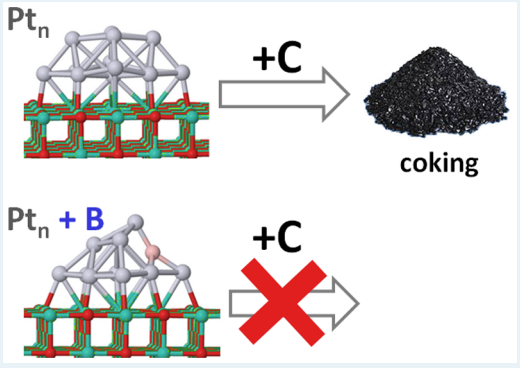

KEYWORDS: *PtB clusters on magnesia, sintering, coking, alloying, density functional theory*

1. INTRODUCTION

Bulk platinum and platinum-based nano- and sub-nano-clusters are excellent catalysts for the processes of (de)hydrogenation and cracking in alkanes.[1−4] Zeolites doped with Pt and other metals have been found to be good catalysts for the dehydrogenation of isobutane to isobutene and propane to propene.[5] In addition, Pt and Pt-based catalysts on hydrotalcite (Mg(Al)O) increase the activity of dehydrogenation of ethane to ethene.[2,6,7] Several studies have shown the catalytic capabilities of stoichiometric and defective MgO(100) surfaces, as well as transition metal catalysts supported on such.[8−12] Successive dehydrogenation to alkynes, and methane production from cracking, can result in coke fouling. These reactions, along with sintering of clusters on the support to form larger islands and monolayers, are the primary sources for deactivation of cluster-catalysts used for dehydrogenation and other processes, e.g. Fischer−Tropsch synthesis.

Others have studied the structure, stability, and activity of Pt clusters supported on graphitic or activated carbon, when such a support itself is borated.[13−15] The effect of boron on bulk Co and Ni catalysts has been well-documented.[16,17] B was also shown to impregnate surfaces and step-sites of Co and Ni, starting from octahedral or nearly square planar geometries. The formation of the surface alloy with square planar B is accompanied by the p4g surface reconstruction. This effect is analogous to that of C on Co and Ni. For both carbides and borides, the effect was recently explained by the acquisition of the local aromaticity in the M_4B or M_4C units on the surface.[18] Both B and C have strong affinities to those metals. When Co and Ni surfaces are decorated with B, the preferred binding sites of C are blocked and adsorption to secondary sites are reduced, due to changes in the surface's electronic structure. Hence, both the initiation of coking and its resulting accumulation are blocked. B-promoted catalysts have significantly extended lifetimes, without a loss of activity.[16] The effect of B on transition metal cluster catalysts has previously not been investigated, and it is unknown whether it can act as coke *antagonist*.

Mixed metal−boron clusters in the gas phase have been studied without an eye toward any practical application.[19,20] Neutral pure metal clusters typically are in a 3D globular configuration. This is due to the delocalized nature of bonding in metal clusters, and delocalized overlap is optimal in such shapes. This is a result of the electron-deficient nature of the metal atoms, coupled with the small cluster size, that prevents the formation of classical metallic or 2c−2e covalent bonds. For some elements, such as Au, where relativistic effects become significant or in some charged clusters, like Pt_5^-, the s- and p-AOs get recruited into the valence shell, sometimes leading to the formation of planar clusters with a partially covalent character of chemical bonding.[11,21] On the other hand, when

Received: March 15, 2015
Published: August 17, 2015

DOI: 10.1021/acscatal.5b01513
ACS Catal. 2015, 5, 5719−5727

clusters of Al (globular when composed only of Al atoms) were doped with B, they were shown to undergo notable structural transformations.[19] The presence of just one or two B atoms was enough to make the clusters flat or nearly flat. Increasing concentration of B leads consistently to a preference for planar structures. This was shown to be due to the appearance of more traditional covalent bonds in the clusters. Unlike delocalized metallic bonding, covalent bonds are directional, resulting in particular atomic coordinations. At the opposite extreme, clusters of pure B are all planar or nearly planar, due primarily to the presence of covalent 2 center−2 electron bonds that are reinforced by 2-fold (σ- and π-) aromaticity in 2D.[22]

The effect of B on the morphology and electronic properties on gas-phase and surface-deposited Pt clusters is undetermined. Importantly, the effects on catalyst deactivation have not been previously studied. It is unknown whether B will present the same benefits as it does on metal surfaces. In this paper, the above questions are addressed using a simple model system: a few representative small Pt clusters deposited on a, structurally simple, magnesia support.

2. METHODS

Calculations for surface-supported clusters were performed using the plane-wave density functional theory (PW-DFT) package *Quantum Espresso*,[24] employing ultrasoft pseudopotentials and the Perdew−Burke−Ernzerhof (PBE) functional.[23−27] The cutoff energies for the basis set and the density were chosen to be 435 and 4350 eV, respectively; these were found to lead to good convergence. All PW-DFT calculations were spin-unrestricted. The MgO(100) surface was modeled as a slab with 3 × 3 × 3 unit cells per supercell with a 1 × 1 × 1 Monkhorst−Pack grid and shifts in k_x and k_y, when the deposited clusters were small (2−6 atoms). The vacuum separation between the top of the surface and the bottom of the repeating image in z was about 12.5 Å. Additional calculations with Pt_{13} supported on magnesia were performed in an extended 4 × 4 × 3 unit cell, to avoid the cluster−cluster interactions. Only the stoichiometric surface was considered in this study due to its structural simplicity, and because it is known that clusters of Pt and Pd preferentially avoid O vacancies, unlike clusters of e.g. Au.[10,28−31] Spin-polarized calculations with fixed multiplicity were performed for gas-phase clusters using the B3LYP,[32−34] PBE, and MP2[35−40] levels of theory with the aug-cc-pVTZ+ECP basis set[41,42] implemented in *Gaussian 09*.[43] Such calculations were used to confirm adequate performance of PW-DFT simulations. Specifically, the effect of basis set was checked, and B3LYP and MP2 were used to check the need for the exact exchange, and the dynamic electron correlation, respectively. Results were found to agree across different theoretical methods, as shown in the Supporting Information. Data presented in the main text was obtained with PW-DFT, for consistency. Molecular orbitals (MOs) were plotted at the Γ-point, using the postprocessing module in *Quantum Espresso*. The search for the global minimum structures in the gas phase was done using the Gradient Embedded Genetic Algorithm (GEGA)[44,45] at UPBE/LANL2DZ-ECP,[46−49] and also the Adaptive Force Field-assisted Coalescent Kick (AFFCK) method recently introduced by Zhai et al.[50] Global minima searches for the supported clusters were done *per manum*, using the gas phase local minima as a guide. GEGA and AFFCK produced a highly diverse population of 2D and 3D local minima structures, which were then oriented in several different ways on the support, to act as starting configurations in the search for the global minimum. To note, there are inherent deficiencies in this process and it is adopted only as a compromise to the tremendous computational cost of performing an advanced search for the global minima of deposited clusters; these issues are currently being addressed in a forthcoming publication on an improved AFFCK method to do global optimization of clusters on surfaces. For the larger Pt clusters, the full global optimization was not attempted, and instead, structures reported in the literature were used as a starting point, as described in the corresponding section.

3. RESULTS AND DISCUSSION

3.1. Doping of Small Pt Clusters with Carbon and Boron. We start the discussion from the smaller clusters, containing 4−6 atoms, for which more thorough calculations could be afforded, and the electronic structure analysis produces a very clear picture. The discussion is then extended first to even smaller clusters, and then also larger and likely more practically relevant clusters. The latter larger-size regime can be addressed only schematically due to computational limitations.

Given the small cluster sizes presented herein, five or six atoms at most, it is an open question whether to view the doping as a decoration or a substitution. Both comparisons are presented below. Previously, the authors have shown that Pt_4 takes on a tetrahedral structure in the gas-phase,[30] while neutral Pt_5 is trigonal-bipyramidal.[11] As seen in Figure 1b the addition

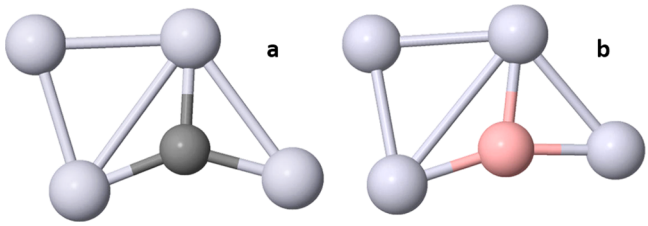

Figure 1. Gas-phase global minima structures of (a) Pt_4C (C_1, ^1A) and (b) Pt_4B (C_1, ^2A). Both elements greatly change the morphology when compared with either Pt_4 or Pt_5. Pt_4C is nearly planar, while Pt_4B is noticeably bent.

of B dramatically deforms the structures, reorganizing the bonding between the Pt atoms. Such distortion and planarization of metal clusters are typically attributed to the onset of partial covalency in bonding.[11,51,52] As a comparison, the Pt cluster was also doped with C (Figure 1a) to determine how the presence of a coke-initiator would affect gas-phase cluster morphology. In both cases, the introduction of main-group chemistry tremendously distorts pure Pt clusters and is done so in a similar way.

The formation energies of the global-minimum gas-phase clusters are shown in Table 1; they are defined as

$$E_{\text{form}} = \frac{E[\text{Pt}_m\text{Y}_n] - mE[\text{Pt}_1] - nE[\text{Y}]}{m + n}$$

It is observed that the introduction of the main-group elements helps to stabilize the gas-phase clusters. This is especially exciting for the case of B, where it will be shown that its presence will aid in reducing sintering caused by Ostwald ripening. For C, the stabilization is the manifestation of the

DOI: 10.1021/acscatal.5b01513
ACS Catal. 2015, 5, 5719−5727

Table 1. Formation Energies (eV/atm) of Pure and Doped Pt Sub-nano-clusters

	Pt_4	Pt_5	Pt_4C	Pt_4B
E_{form}	−2.97[a]	−2.88[b]	−3.97	−3.96

[a]Result taken from ref 35. [b]Result taken from ref 11.

well-known intrinsic affinity to coke. Notice also that C and B have nearly identical effects on cluster stability.

While B deposited on metal interfaces leads to surface reconstruction, the effect on the structures of subnanoclusters is even more pronounced. Previously, the authors have shown that both Pt_4 and Pt_5 undergo morphological modification when attached to MgO.[11,12] For the case of Pt_4 the cluster broadens, with three Pt atoms coordinating to surface O atoms and one Pt atom on top, balancing between metal−metal and metal−oxide bonding.[12] The case of Pt_5 was more striking, with the cluster going planar and standing upright as a result of an induced partial covalency due to large charge-transfer from the support. A similar effect was observed when considering the substitution of one of the Pt atoms with Zn.[11] The situation with B is more complex. The boron-doped cluster (Pt_4B) undergoes morphological changes when deposited on MgO, relative to its gas-phase geometry, as shown in Figure 2. The

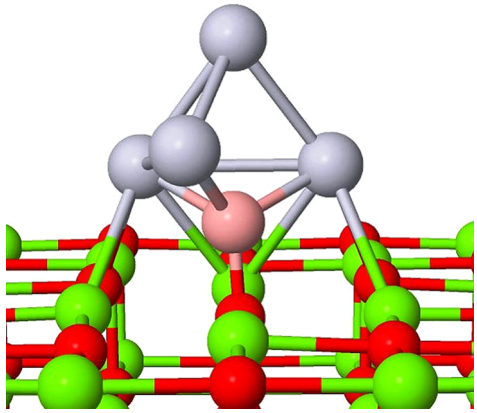

Figure 2. Global minimum structure of Pt_4B on the MgO support.

MgO supported Pt_4B cluster goes from a bent *semiplanar* structure back to a 3D one with B demonstrating a great affinity for surface O atoms, effectively forming a boron oxide anchor.

Note that the discussion focuses on just the single most stable structure in each case. However, the fluxionality of the clusters may play a major role in catalysis,[53,54] and therefore our exclusive focus on global minima needed further justification. We calculated the Boltzmann-weighted average of the most energetically favorable structures, as it was made in previous studies.[30,55] Thus, the Boltzmann probability for *i*th configuration (P_i) was found by taking the Boltzmann distribution of each isomer ($e^{-E_i k_B T}$) divided by the sum of the distributions of all relevant minima:

$$P_i = \frac{e^{-E_i/k_B T}}{\sum e^{-E_i/k_B T}}$$

where E_i is the energy of each low-energy isomer. P_i calculated in this way gives the probability of the given minimum to be occupied at the T of interest. The set of isomers included in this calculation was truncated at the point where no appreciable change in the population distribution was observed upon further expansion of the set, and the high-energy isomers had P_i of less than 10^{-3}. In Table 2 the probabilities P_i of the most relevant local minima are given for Pt_4, Pt_5, and Pt_4B clusters supported on magnesia. These local minima are depicted in the Supporting Information. The characterized lowest-lying isomers are clearly predominant at temperatures up to 1000 K. Therefore, the focus on the global-minimum structures in this study is justified though remains to be an approximation.

3.2. Chemical Bonding Analysis for Pt and PtB Clusters in the Gas Phase and on the Support. B was previously found to significantly distort metallic clusters due to a strong covalent character of boron−metal and boron−boron bonds. Boron, being just prior to carbon in the periodic table, has a similar propensity to hybridize its 2s- and 2p-AOs. In many ways B behaves like C^+, likewise C behaves like B^-. In addition, B is closer in electronegativity to transition metals than C, $\chi_C = 2.54$, $\chi_{Pt} = 2.28$, and $\chi_B = 2.04$ on the Pauling scale. Therefore, B can induce partial covalency also with metals—the indication of this being strong structural distortions away from more metal-like 3D globular shapes, 2sp-hybridization on B, and lack of ionic bonding as judged by atomic charges.[19]

To reiterate, Pt_5 in the gas-phase is trigonal bipyramidal (D_{3h}, quintet) (typical of many all-metal clusters) with the total formation energy of −2.88 eV per atom. Substituting a single Pt atom with B produces the semiplanar Pt_4B structure (Figure 1b) with total formation energy of −3.96 eV per atom. Hence, B substitution acts to dramatically stabilize the cluster. The natural electronic configuration on atoms, as produced by the NBO analysis,[56] shows a significant mixing of 2s and 2p AOs on B: $[core]2s^{1.11}2p^{1.94}$, and s−p−d mixing on Pt, for example the central Pt atom in the structure has the following configuration: $[core]6s^{0.72}5d^{9.07}6p^{0.19}$. NBO analysis further predicts two major resonance structures, for each there are two classical covalent Pt−B bonds populated by ca. 1.7 e, and the Pt atom involved in this bonding is the most hybridized in the cluster. The strong Pt−B bonding in the gas phase cluster is also apparent from the examination of the MOs (see Figure S2, in the SI).

When deposited on the support, B preferentially binds to the surface O atom and the globular structure of the Pt cluster is largely restored. The B−O bond is 1.43 Å, close to those in boron oxide (1.34 and 1.40 Å).[57] From the Bader charge analysis,[58−60] the cluster acquires −0.21 e charge, a smaller charge transfer when compared with −0.73 e and −0.80 e for MgO supported Pt_4 and Pt_5, respectively. The delocalized bonding in this system leads to the globular shape and signals

Table 2. Boltzmann Populations of the Most Stable Pt_4, Pt_5, and Pt_4B Isomers

Pt_4 isomer	P_{300K}	P_{700K}	P_{1000K}	Pt_5 isomer	P_{300K}	P_{700K}	P_{1000K}	Pt_4B isomer	P_{300K}	P_{700K}	P_{1000K}
global min	99.99%	99.38%	96.90%	***global min***	94.83%	76.36%	66.69%	***global min***	99.99%	99.99%	99.99%
2	<0.01%	0.56%	2.59%	**2**	5.16%	21.92%	27.84%	**2**	<0.01%	<0.01%	<0.01%
3	<0.01%	0.05%	0.51%	**3**	0.01%	1.42%	4.10%				
				4	<0.01%	0.29%	1.35%				

DOI: 10.1021/acscatal.5b01513
ACS Catal. 2015, 5, 5719−5727

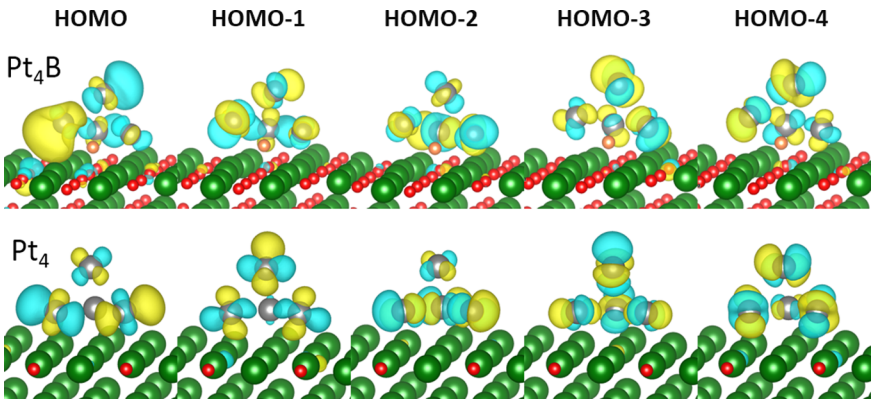

Figure 3. Frontier valence MOs of the MgO-deposited Pt_4 and Pt_4B clusters (density is sampled at the Γ-point). The figure illustrates that the electron density is not depleted from the protruding Pt atoms upon B doping, those leaving those sites available for substrate binding. The noticeable difference is in the degree of the spd-hybridization on the Pt atoms in the doped cluster.

the reduced spd-hybridization on Pt atoms. Figure 3 shows the frontier valence MOs of the deposited Pt_4B and Pt_4, demonstrating that the valence electron density is not much depleted from the protruding Pt atoms—an effect that could deactivate the catalyst. The HOMO−LUMO gap is increased upon alloying with B by a few tenths of electronvolt, indicated by plots of the total density of states (DOS) shown in Figure 4.

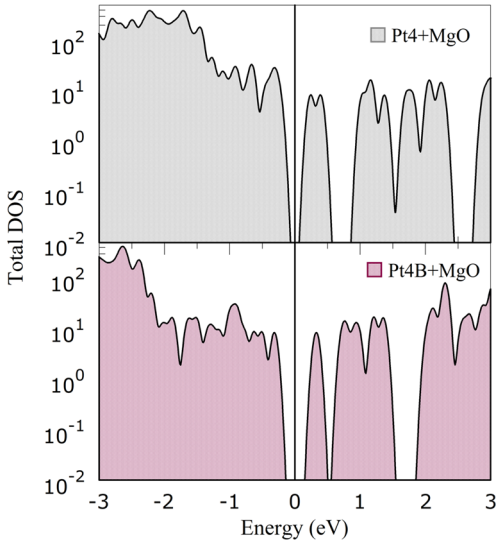

Figure 4. Total density of states (DOS) energies are zeroed to the Fermi energy (labeled by a dark vertical line) of the given system. The opening of the HOMO−LUMO gap is seen for the borated cluster.

The subtle shifts in the energies of states upon alloying with B are expected to have some effect on catalytic activity. However, when alloying bulk metal catalysts with B was done in the past,[16,17] the catalytic activity was not harmed, and the effect reduced to that of a selected poisoning. We do not yet address this reactivity aspect here, beyond the questions of stability. The impact of these changes in the electronic structure on cluster stability is examined in the next section.

3.3. Deactivation−Resistance of Potential Cluster Catalysts from B Doping. Cluster catalyst deactivation via sintering can proceed as a result of Ostwald ripening, particle coalescence, or some combination of the two. In order to make a qualitative comparison between the sintering susceptibilities of pure and B-doped clusters, two quantities are critical: the energy for the monomer to dissociate away from the clusters and the adsorption energy of the cluster to the support. For Ostwald ripening, monomers must dissociate from a cluster, migrate on the support, and integrate into larger clusters. Hence, the propensity to sinter in this way depends strongly on cluster dissociation energies, and on monomer mobility. In the present case, the mobility of Pt monomers is governed by the PES presented by the support. To move from minima to minima (i.e., from one O atom to the next) it must overcome a barrier of ∼0.6 eV;[11,12] this can be accomplished at higher temperatures relevant to catalysis. The monomer motion also does not depend on alloying with B. The energy penalty to reverse ripen, i.e. for a monomer to dissociate from the cluster so that it can sinter to a larger cluster, is called the sintering energy (E_S) and will differ for the pure and B-doped clusters. E_s is defined as

$$E_S = E[Pt_mB_n + MgO] + E[MgO] - E[Pt_{m-1}B_n + MgO] - E[Pt_1 + MgO]$$

Where, in the present case, m = 4 or 5 and n = 0 or 1.

The particle coalescence mechanism involves migration of clusters on the support and their merger into larger nanoparticles. This process is most facile when cluster adsorption energies (E_{ads}) and the barriers for cluster migration from site to site are small. As a first-order approximation, only E_{ads} is considered and it is defined by

$$E_{ads}[Pt_mB_n] = E[Pt_mB_n + MgO] - E[MgO] - E_{gas}[Pt_mB_n]$$

In Table 3, the sintering energy penalties and adsorption energies are presented for Pt_4, Pt_4B, and Pt_5. Again, the dissociation channels considered were from the global minima of the deposited clusters, resulting in a Pt monomer attached to the highest-affinity site of the support and the global minima of

Table 3. Sintering Energy Penalties, to Form a Pt Monomer from a Given Supported Cluster, and Adsorption Energies of the Cluster to the MgO Support (eV)

	Pt_4	Pt_4B	Pt_5
E_S	−1.80	−2.17	−1.48
E_{ads}	−3.75	−4.20	−3.66

DOI: 10.1021/acscatal.5b01513
ACS Catal. 2015, 5, 5719−5727

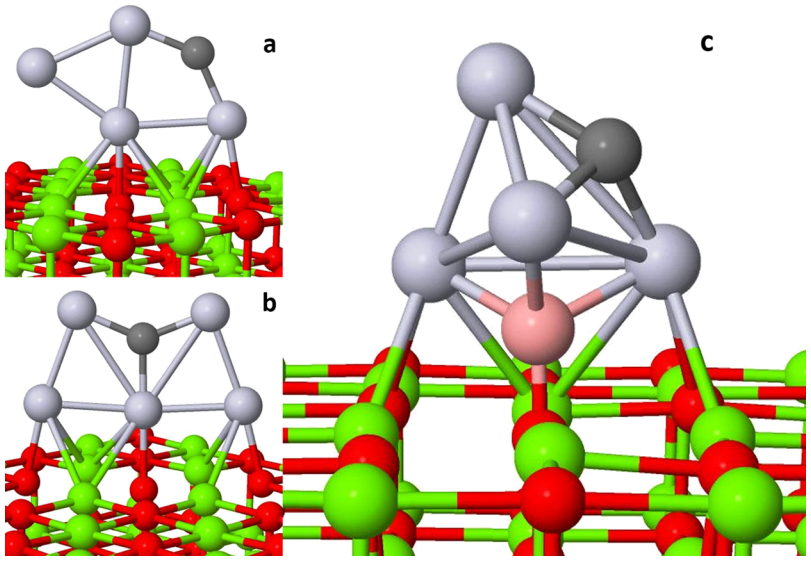

Figure 5. Global minima structures of surface-mounted coked Pt-based subnanoclusters: (a) Pt_4C, (b) Pt_5C, and (c) Pt_4BC.

the supported Pt_3, Pt_3B, and Pt_4 cluster, respectively. Adding B to Pt clusters lowers E_S by ∼0.5 eV, as compared with either Pt_4 or Pt_5. This indicates that the process of Ostwald ripening will be reduced for the B-doped Pt clusters. Likewise E_{ads} is lowered by ∼0.5 eV, relative to the pure Pt cases. This suggests that additionally sintering via particle coalescence becomes less likely upon doping. Of course, these effects may be specific to the system under consideration, and not universal. However, the intracluster stabilization when B is added is not surprising based on earlier findings of the covalent nature of metal−boron interactions and the strong effect of B on cluster morphology. Thus, it seems likely that the above sintering-resistant consequences could hold up for metal clusters of many different sizes and compositions. To an extent this is further addressed below. It is noted that the MgO(110) surface presents a very level interface. Other oxide surfaces, such as $TiO_2(100)$ and α-$Al_2O_3(0001)$, are more corrugated—having protruding O atoms. Given that B binds covalently to the surface O atoms and forms an anchor on MgO, it can reasonably be argued that under-coordinated protruding O atoms of other supports may provide even better candidates to further restrain Pt−B clusters. Therefore, the above results present the first indications that boron-doping can render Pt-based clusters resistant to sintering on oxide supports.

Importantly, now the issue of reducing the propensity for coke deposition is considered. The full process of coking is complicated, and involves the initiation of C binding to multiple sites, and then growth from those sites to form graphitic and other forms of bulk-like C on the catalyst. We consider only one rudimentary step of this process: binding of the first C atom to the cluster, needed to initiate the process of coking. Studying the processes in its great complexity is beyond the scope of this work. In Figure 5, the global minima structures for Pt_4C, Pt_5C, and Pt_4BC are shown. It is noted that the bonding arrangement of Pt_4C on MgO is only mildly modified compared with its gas-phase structure. The C atom is slightly displaced away from the center of mass of the cluster and preferring to not directly interact with the surface interface, allowing more of the Pt atoms to coordinate with surface O atoms. The morphology of the C-bound structure is quite different from either Pt_4 + MgO or Pt_4B + MgO, being more in line with Pt_5 + MgO and especially Pt_4Zn + MgO.[11,12] C deposited on Pt_5 has only a mild effect on that cluster's morphology—a comparison to Pt_6 is beyond the scope of the present work. Similarly, C does little to change the structure of Pt_4B + MgO. Overall, the primary role of C is to block substrate binding sites, leading to its deactivation.

The sticking or binding energy (E_B) of C to a supported cluster is defined as

$$E_B[C] = E[Pt_mB_nC + MgO] - E[Pt_mB_n + MgO] - E_{gas}[C]$$

again, in the present case, m = 4 or 5 and n = 0 or 1. The gaseous form of C can be questioned, and it depends on the particular reaction being catalyzed. However, since in this work only comparisons between different clusters to each other are made, and the absolute coking energetics are not addressed, the generic reference in the equation above is acceptable. Table 4 presents the carbon sticking energies for the Pt_4, Pt_4B, and Pt_5 clusters supported on MgO.

Table 4. Binding Energies of Carbon to the Various MgO Supported Pt-Based Clusters (eV)

	Pt_4	Pt_4B	Pt_5
$E_B[C]$	−4.76	−3.34	−5.90

The binding energies are quite deep, due to the fact that only the ideal case of C desorption to the gas-phase is being considered. However, remembering the approximation spelled out in the previous paragraph, and considering only the trend between different clusters, it is observed that the addition of only a single B atom into the cluster reduces the attachment energy of C by roughly ∼2.0 eV, whether comparing to Pt_4 or Pt_5. Deposited Pt_4B is notably more resilient against carbon deposits. This effect may be attributed to the changed nucelophilicity of the Pt sites in the borated cluster, due to the modification of charge transfer from the support, discussed above. The result may promise that a larger nanoparticle, decorated with a reasonable amount of B, could act as a catalyst nearly completely resistant to coke deactivation.

DOI: 10.1021/acscatal.5b01513
ACS Catal. 2015, 5, 5719−5727

3.4. Effect of Cluster Size on the Role of B in Stabilization of Deposited Pt Clusters. It is well-known that the properties of the subnanometer clusters change discontinuously with the size. It is therefore important to see whether or not the exciting effects described above hold a promise to be universal, or are specific to the considered smaller clusters. We therefore have additionally analyzed the effect of B doping on the smaller Pt_3, and significantly larger Pt_{13} cluster, toward the deactivation by both sintering and coking. Pt_{13} is considered as being representative of highly dispersed platinum catalysts with particle size close to 1 nm,[61] and therefore brings us closer to the realistic nanoparticle regime. We note, however, that in many cases the subnanometer metallic clusters made of only a few atoms were shown to be the true actors in catalysis.[62−64] Therefore, it is questionable whether the stabilization of large or small clusters is more critical for the real catalyst lifetime. While this remains an open question here, we address the chosen systems, representative of the smaller and the larger regimes. It must be emphasized that the size of the system under study is a very important limiting factor to perform first-principles calculations.

The ground-state Pt_3 cluster in gas phase is a slightly distorted triangle (C_s, $^3A_1$), in agreement with previous works.[65,66] The substitution of one Pt atom on Pt_3 by B gives rise to an isosceles triangle (C_s, $^2A'$). The effect of substituting one Pt atom by carbon is similar (the resultant spectroscopic state is C_s, $^1A'$). As in the case of Pt_4 and Pt_5, the introduction of the main-group element increases the cluster formation energies (Table 5).

Table 5. Formation Energies of Pure and Doped Pt Sub-nano-clusters (eV/atm)

	Pt_2	Pt_3	Pt_2C	Pt_2B
E_{form}	−0.94	−1.21	−1.82	−1.68

When deposited on MgO, Pt_3 becomes preferentially linear, maximizing the interaction with the support O atoms. Pt_2B, however, is highly deformed, and boron reaches down to form a strong boron oxide anchor (Figure 6a and b). In Table 6, the calculated adsorption energies and the sintering energies are shown. Observe that B doping reduces the propensity to sinter, according to the energetics criteria introduced in this work. The sintering energies are lowered, indicating reduced Ostwald ripening. At the same time, the adsorption energies are lowered too, making the particle migration and coalescence also less probable. The carbon binding energies are also given in Table 6, and the corresponding structures of Pt_2C, Pt_3C, and Pt_2BC are shown in Figure 6c−e. Again, the introduction of boron as a dopant weakens the interaction of the hole cluster with carbon, and that again suggests the improvement of resistance to coking. Observe that, as in the clusters analyzed in the previous section, carbon clearly avoids the direct interaction with the surface. Thus, for smaller clusters of Pt, the promising effect of B-doping holds true.

Table 6. Sintering Energy Penalties, to Form a Pt Monomer from a Given Supported Cluster, Adsorption Energies of the Cluster to the MgO Support, and C binding energies (eV)

	Pt_2	Pt_2B	Pt_3
E_S	−0.60	−2.84	−1.56
E_{ads}	−1.78	−3.99	−2.14
E_B[C]	−7.29	−5.84	−7.54

The representative larger platinum cluster that we consider is Pt_{13}. Its gas-phase global-minimum was reported to be the so-called DIS isomer,[67,68] it is a triplet (Figure 7). In this work, we directly reused this previously reported isomer. For Pt_{12}, the structure was obtained by removal of one Pt atom from Pt_{13}, relaxing the structures thus produced, and then choosing the lowest-energy isomer. $Pt_{12}B$, and $Pt_{12}C$ were obtained by substituting one Pt atom in Pt_{13} with B/C, optimizing the structures and also choosing the lowest-energy isomers. Note that this is not a true global optimization, and therefore, results presented here are merely suggestive. The pure Pt clusters have fairly globular shapes, whereas the introduction of B or C gives rise to significantly distorted $Pt_{12}B$, and $Pt_{12}C$ (Figure 7). Note

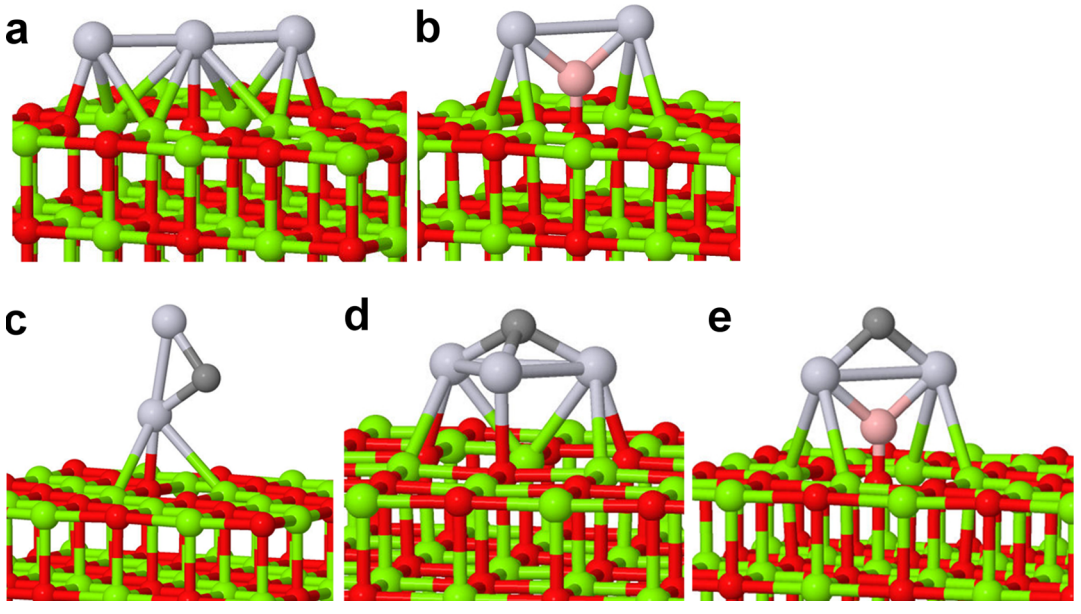

Figure 6. Global minimum structures of (a) Pt_3, (b) Pt_2B, (c) Pt_2C, (d) Pt_3C, and (e) Pt_2BC on the MgO support.

DOI: 10.1021/acscatal.5b01513
ACS Catal. 2015, 5, 5719−5727

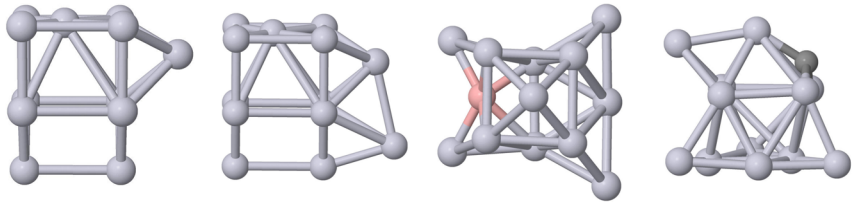

Figure 7. From the left to the right, the optimized lowest-energy structures of Pt_{12}, Pt_{13}, $Pt_{12}B$, and $Pt_{12}C$ used in this work.

that the same effect is found in the Pt_4/Pt_5 clusters. In case of larger clusters, further dramatic distortion can be expected when more B or C is added, but this will be the subject of further studies. The formation energies shown in Table 7 reflect the stabilization of these metallic nanoclusters upon introduction of both B and C, though the stabilization is not as pronounced as for the smaller species, probably because of the smaller B(C)/Pt ratio.

Table 7. Formation Energies (eV/atm) of Pure and Doped Pt Sub-nano-clusters

	Pt_{12}	Pt_{13}	$Pt_{12}C$	$Pt_{12}B$
E_{form}	−3.62	−3.68	−3.89	−3.90

For Pt_{13} deposited on magnesia, we hypothesize a flat biplanar structure with the maximal interaction with the support (Figure 8a). This structure has not been previously reported, but the reason for our hypothesis is as follows. A recent work[69] showed that the most stable configuration for Pd_{13} on magnesia is the one shown in Figure 8a. When deposited on gamma-alumina, Pd_{13} and Pt_{13} were found to form the same isomers.[70] Also on titania, pure and mixed Pt and Pd clusters adopt identical structures.[30] In view of this analogous behavior, we assume that Pt_{13} on MgO should look like Pd_{13} on MgO (i.e., the structure in Figure 8a). For $Pt_{12}C$ and $Pt_{12}B$, the considered isomers were generated by substituting each Pt atom in the Pt_{13} ground-state isomer with C/B. The resulting most stable $Pt_{12}B$ structure is shown in Figure 8b. In this particular case, boron is not found interacting directly with the surface. Instead, it is surrounded by platinum atoms, maximizing the number of bonds. The calculated adsorption energies and the sintering energies, shown in Table 8, reveal that the effect of boron doping in such a big cluster is clearly dissipated. Indeed, these calculated energies are similar to the energies calculated for the Pt_{12} cluster and close to the energies corresponding to Pt_{13} nanoparticle.

Table 8. Sintering Energy Penalties to Form a Pt Monomer from a Given Supported Cluster, Adsorption Energies of the Cluster to the MgO Support, and C Binding Energies to the Various MgO-Supported, Pt-Based Clusters (eV)

	Pt_{12}	$Pt_{12}B$	Pt_{13}
E_S	−1.91	−1.87	−2.30
E_{ads}	−4.35	−4.42	−4.47
$E_B[C]$	−7.29	−6.72	−7.03

Nevertheless, boron has a positive impact on the reduced propensity for coke deposition. In Figure 8c–e, the most stable structures found for $Pt_{12}C$, $Pt_{13}C$, and $Pt_{12}BC$ are shown. C persistently avoids the direct interaction with the support. From the carbon binding energies calculated for Pt_{12}, Pt_{13}, and $Pt_{12}B$ (Table 8), it is evident that the presence of boron discourages considerably the binding of C. This effect, however, is smaller than in previous cases, indicating that the boron concentration is an important factor influencing these properties, and a lever in catalyst design for selectivity and against coking.

We believe that the results shown in this work open the possibility of improving platinum catalysts in different ways. On the one hand, since the introduction of boron improves the sintering resistance, these subnanometer clusters could be used

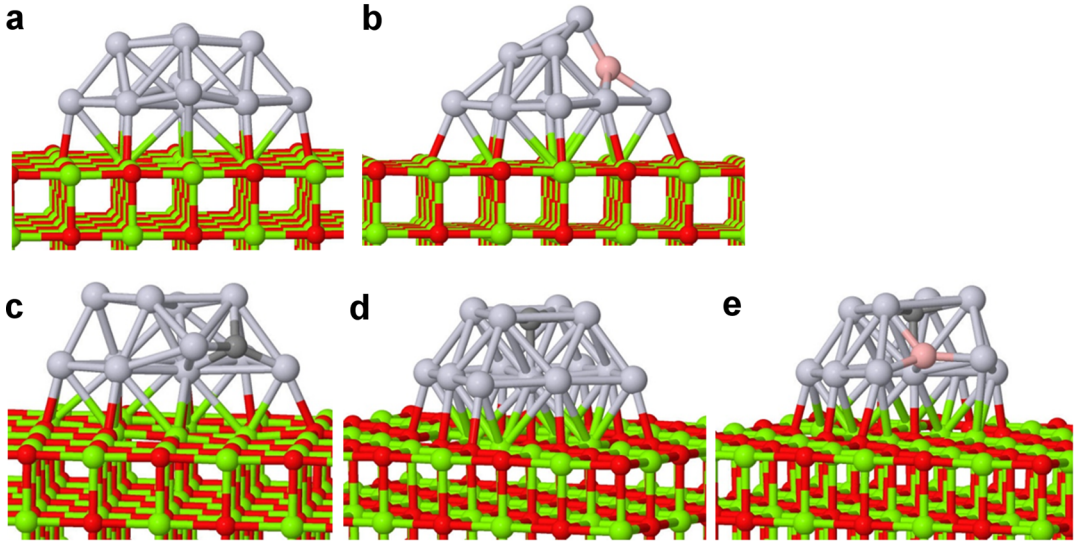

Figure 8. Considered isomers found for (a) Pt_{13}, (b) $Pt_{12}B$, (c) $Pt_{12}C$, (d) $Pt_{13}C$, and (e) $Pt_{12}BC$ on MgO.

DOI: 10.1021/acscatal.5b01513
ACS Catal. 2015, 5, 5719–5727

directly as catalysts, with no need of using bigger nanoparticles, supporting in this way a "greener" and cheaper chemistry. In this vein, the next step would be to analyze their catalytic activity for (de)hydrogenation of alkanes. On the other hand, the fact that the presence of boron decreases the affinity toward carbon, suggest that solid solutions of platinum, where boron is located in interstitial holes, could also benefit from main group element impurities and a highly coking resistance catalyst might be developed in this line. Thus, the selectivity of catalytic dehydrogenation might be improved. Finally, we would like to point out a related effect found in B-doped Pd catalysts,[71,72] where the presence of surface and subsurface B dramatically improves the selectivity for typical partial hydrogenation reactions.

4. CONCLUSIONS

This DFT study suggests that B-doping of MgO-supported nano- and sub-nano-clusters of Pt can lead to the reduction in the chance for catalyst deactivation. At least from the simple and small models used, B seems to play a 3-fold role. First, it increases the sintering energy penalty for a Pt atom to dissociate off the clusters, thus reducing the rate of sintering by Ostwald ripening. However, B often does not present itself to the surface of the cluster, still leaving Pt atoms as the sites for the substrate of the catalyzed reaction. Second, B anchors the cluster to the support, increasing the adsorption energy and thus decreasing the odds of particle migration and coalescence. This effect is cluster size-dependent, however, and connected to whether or not the B−O bonds form to anchor the cluster to the support. Finally, B greatly reduces the C sticking (or binding) energy to the clusters of all considered sizes. The effect of discouraged C binding is rooted in the altered charge distribution and the nucleophilicity of the Pt atoms serving as C-binding sites in the deposited borated clusters. This latter result suggests that the initiation of coking on deposited clusters of Pt can be greatly reduced by alloying the clusters with B. Note that the actual process of coking is complicated and is not considered in this model study. Neither is the effect of alloying Pt with B on the catalytic activity toward dehydrogenation of alkanes, which is our process of interest, addressed. However, the findings presented here suggest a greater selectivity of dehydrogenation. This work suggests, for the first time, that the effect of B may also serve a prominent role in cluster catalysts.

■ ASSOCIATED CONTENT

Supporting Information

The Supporting Information is available free of charge on the ACS Publications website at DOI: 10.1021/acscatal.5b01513.

Calculated ab initio data for gas phase clusters, valence MO diagrams for gas phase, and deposited clusters; different Pt_4, Pt_5, and Pt_4B isomers (PDF)

■ AUTHOR INFORMATION

Corresponding Author

*E-mail: ana@chem.ucla.edu.

Notes

The authors declare no competing financial interest.

■ ACKNOWLEDGMENTS

The authors acknowledge support from the Air Force Office of Scientific Research under AFOSR BRI Grant FA9550-12-1-0481. Computational resources were provided by the UCLA-IDRE cluster. A portion of the research was performed using EMSL, a national scientific user facility sponsored by the Department of Energy's Office of Biological and Environmental Research and located at Pacific Northwest National Laboratory.

■ REFERENCES

(1) Bhasin, M.; McCain, J.; Vora, B.; Imai, T.; Pujado, P. *Appl. Catal., A* **2001**, *221*, 397−419.
(2) Galvita, V.; Siddiqi, G.; Sun, P.; Bell, A. *J. Catal.* **2010**, *271*, 209−219.
(3) Burch, R.; Garla, L. *J. Catal.* **1981**, *71*, 360−372.
(4) Weckhuysen, B.; Schoonheydt, R. *Catal. Today* **1999**, *51*, 223−232.
(5) De Cola, P. L.; Glaser, R.; Weitkamp, J. *Appl. Catal., A* **2006**, *310*, 205−206.
(6) Sun, P.; Siddiqi, G.; Vining, W.; Chi, M.; Bell, A. *J. Catal.* **2011**, *282*, 165−174.
(7) Siddiqi, G.; Sun, P.; Galvita, V.; Bell, A. *J. Catal.* **2010**, *274*, 200−206.
(8) Henrich, V.; Cox, P. *The Surface Science of Metal Oxides*; Cambridge University Press, Cambridge, England, 1996.
(9) Campbell, C. T. *Acc. Chem. Res.* **2013**, *46*, 1712−1719.
(10) Yoon, B.; Hakkinen, H.; Landman, U.; Worz, A. S.; Antonietti, J. M.; Abbet, S.; Judai, K.; Heiz, U. *Science* **2005**, *307*, 403−407.
(11) Shen, L.; Dadras, J.; Alexandrova, A. N. *Phys. Chem. Chem. Phys.* **2014**, *16*, 26436−26442.
(12) Dadras, J.; Shen, L.; Alexandrova, A. N. *J. Phys. Chem. C* **2015**, *119*, 6047−6055.
(13) Acharya, C. K.; Sullivan, D. I.; Turner, C. H. *J. Phys. Chem. C* **2008**, *112*, 13607−13622.
(14) Acharya, C. K.; Turner, C. H. *J. Phys. Chem. B* **2008**, *110*, 17706−17710.
(15) Sine, G.; Duo, I.; Roustom, E. I.; Foti, G.; Comninellis, Ch. *J. Appl. Electrochem.* **2006**, *36*, 847−862.
(16) Xu, J.; Saeys, M. *J. Catal.* **2006**, *242*, 217−226.
(17) Tan, K. F.; Chang, J.; Borgna, A.; Saeys, M. *J. Catal.* **2011**, *280*, 50−59.
(18) Nandula, A.; Trinh, Q. T.; Saeys, M.; Alexandrova, A. N. *Angew. Chem., Int. Ed.* **2015**, *54*, 5312−5316.
(19) Huynh, M.; Alexandrova, A. N. *J. Phys. Chem. Lett.* **2011**, *2*, 2046−2051.
(20) Romanescu, C.; Galeev, T. R.; Li, W.-L.; Boldyrev, A. I.; Wang, L.-S. *Acc. Chem. Res.* **2013**, *46*, 350−358.
(21) Lee, H. M.; Kim, K. S. *Chem. - Eur. J.* **2012**, *18*, 13203−13207.
(22) Alexandrova, A. N.; Boldyrev, A. I.; Zhai, H.-J.; Wang, L.-S. *Coord. Chem. Rev.* **2006**, *250*, 2811.
(23) Perdew, J.; Burke, K.; Ernzerhof, M. *Phys. Rev. Lett.* **1996**, *77*, 3865−3868.
(24) Giannozzi, P.; Baroni, S.; Bonini, N.; Calandra, M.; Car, R.; Cavazzoni, C.; Ceresoli, D.; Chiarotti, G.; Cococcioni, M.; Dabo, I.; Dal Corso, A.; de Gironcoli, S.; Fabris, S.; Fratesi, G.; Gebauer, R.; Gerstmann, U.; Gougoussis, C.; Kokalj, A.; Lazzeri, M.; Martin-Samos, L.; Marzari, N.; Mauri, F.; Mazzarello, R.; Paolini, S.; Pasquarello, A.; Paulatto, L.; Sbraccia, C.; Scandolo, S.; Sclauzero, G.; Seitsonen, A. P.; Smogunov, A.; Umari, P.; Wentzcovitch, R. M. *J. Phys.: Condens. Matter* **2009**, *21*, 395502−395520.
(25) Kohn, W.; Sham, L. *Phys. Rev.* **1965**, *140*, A1133−A1138.
(26) Vanderbilt, D. *Phys. Rev. B: Condens. Matter Mater. Phys.* **1990**, *41*, 7892−5.
(27) Burke, K.; Werschnik, J.; Gross, E. *J. Chem. Phys.* **2005**, *123*, 062206−062214.
(28) Zhang, J.; Alexandrova, A. N. *J. Chem. Phys.* **2011**, *135*, 174702.
(29) Zhang, J.; Alexandrova, A. N. *J. Phys. Chem. Lett.* **2012**, *3*, 751−754.
(30) Ha, M.-A.; Dadras, J.; Alexandrova, A. N. *ACS Catal.* **2014**, *4*, 3570−3580.

DOI: 10.1021/acscatal.5b01513
ACS Catal. 2015, 5, 5719−5727

(31) Zhang, J.; Alexandrova, A. N. *J. Phys. Chem. Lett.* **2013**, *4*, 2250−2255.
(32) Becke, A. D. *J. Chem. Phys.* **1993**, *98*, 5648−52.
(33) Lee, C.; Yang, W.; Parr, R. G. *Phys. Rev. B: Condens. Matter Mater. Phys.* **1988**, *37*, 785−89.
(34) Miehlich, B.; Savin, A.; Stoll, H.; Preuss, H. *Chem. Phys. Lett.* **1989**, *157*, 200−06.
(35) Moller, C.; Plesset, M. S. *Phys. Rev.* **1934**, *46*, 618−622.
(36) Headgordon, M.; Pople, J. A.; Frisch, M. J. *Chem. Phys. Lett.* **1988**, *153*, 503−506.
(37) Saebo, S.; Almlof, J. *Chem. Phys. Lett.* **1989**, *154*, 83−89.
(38) Frisch, M. J.; Head-Gordon, M.; Pople, J. A. *Chem. Phys. Lett.* **1990**, *166*, 275−280.
(39) Frisch, M. J.; Head-Gordon, M.; Pople, J. A. *Chem. Phys. Lett.* **1990**, *166*, 281−289.
(40) Head-Gordon, M.; Head-Gordon, T. *Chem. Phys. Lett.* **1994**, *220*, 122−128.
(41) Peterson, K.; Puzzarini, C. *Theor. Chem. Acc.* **2005**, *114*, 283−296.
(42) Figgen, D.; Rauhut, G.; Dolg, M.; Stoll, H. *Chem. Phys.* **2005**, *311*, 227−244.
(43) Frisch, M.; Trucks, G.; Schlegel, H.; Scuseria, G.; Robb, M.; Cheeseman, J.; Scalmani, G.; Barone, V.; Mennucci, B.; Petersson, G. A.; Nakatsuji, H.; Caricato, M.; Li, X.; Hratchian, H. P.; Izmaylov, A. F.; Bloino, J.; Zheng, G.; Sonnenberg, J. L.; Hada, M.; Ehara, M.; Toyota, K.; Fukuda, R.; Hasegawa, J.; Ishida, M.; Nakajima, T.; Honda, Y.; Kitao, O.; Nakai, H.; Vreven, T.; Montgomery, J. A., Jr.; Peralta, J. E.; Ogliaro, F.; Bearpark, M.; Heyd, J. J.; Brothers, E.; Kudin, K. N.; Staroverov, V. N.; Kobayashi, R.; Normand, J.; Raghavachari, K.; Rendell, A.; Burant, J. C.; Iyengar, S. S.; Tomasi, J.; Cossi, M.; Rega, N.; Millam, J. M.; Klene, M.; Knox, J. E.; Cross, J. B.; Bakken, V.; Adamo, C.; Jaramillo, J.; Gomperts, R.; Stratmann, R. E.; Yazyev, O.; Austin, A. J.; Cammi, R.; Pomelli, C.; Ochterski, J. W.; Martin, R. L.; Morokuma, K.; Zakrzewski, V. G.; Voth, G. A.; Salvador, P.; Dannenberg, J. J.; Dapprich, S.; Daniels, A. D.; Farkas, Ö.; Foresman, J. B.; Ortiz, J. V.; Cioslowski, J.; Fox, D. J. *Gaussian 09*, Revision D.01; Gaussian, Inc., Wallingford CT, 2009.
(44) Alexandrova, A. N. *J. Phys. Chem. A* **2010**, *114*, 12591−12599.
(45) Alexandrova, A. N.; Boldyrev, A. I. *J. Chem. Theory Comput.* **2005**, *1*, 566.
(46) Dunning, T. H.; Hay, P. J. Gaussian Basis Sets for Molecular Calculations. *Modern Theoretical Chemistry*; Schaefer, H. F., III, Ed.; Plenum: New York, 1977; Vol. 3, pp 1−28.
(47) Hay, P.; Wadt, W. *J. Chem. Phys.* **1985**, *82*, 270−283.
(48) Wadt, W.; Hay, P. *J. Chem. Phys.* **1985**, *82*, 284−298.
(49) Hay, P.; Wadt, W. *J. Chem. Phys.* **1985**, *82*, 299−310.
(50) Zhai, H.; Ha, M.-A.; Alexandrova, A. N. *J. Chem. Theory Comput.* **2015**, *11*, 2385−2393.
(51) Alexandrova, A. N. *Chem. Phys. Lett.* **2012**, *533*, 1−5.
(52) Alexandrova, A. N.; Nayhouse, M. J.; Huynh, M. T.; Kuo, J. L.; Melkonian, A. V.; Chavez, G.; Hernando, N. M.; Kowal, M. D.; Liu, C.-P. *Phys. Chem. Chem. Phys.* **2012**, *14*, 14815−14821.
(53) Wang, Y.; Mei, D.; Glezakou, V.; Li, J.; Rousseau, R. *Nat. Commun.* **2015**, *6*, 6511−6518.
(54) Li, J.; Yin, D.; Chen, C.; Li, Q.; Lin, L.; Sun, R.; Huang, S.; Wang, Z. *J. Appl. Phys.* **2015**, *117*, 085303−085308.
(55) Dadras, J.; Shen, L.; Alexandrova, A. *J. Phys. Chem. C* **2015**, *119*, 6047−6055.
(56) Glendening, E. D.; J. K. Badenhoop, Reed, A. E.; Carpenter, J. E.; Bohmann, J. A.; Morales, C. M.; Weinhold, F. *NBO 5.0.*; Theoretical Chemistry Institute, University of Wisconsin, Madison, 2001.
(57) Gurr, G. E.; Montgomery, P. W.; Knutson, C. D.; Gorres, B. T. *Acta Crystallogr., Sect. B: Struct. Crystallogr. Cryst. Chem.* **1970**, *B26*, 906−915.
(58) Tang, W.; Sanville, E.; Henkelman, G. *J. Phys.: Condens. Matter* **2009**, *21*, 084204−084210.
(59) Sanville, E.; Kenny, S.; Smith, R.; Henkelman, G. *J. Comput. Chem.* **2007**, *28*, 899−908.
(60) Henkelman, G.; Arnaldsson, A.; Jonsson, H. *Comput. Mater. Sci.* **2006**, *36*, 354−360.
(61) Chizallet, C.; Raybaud, P. *Catal. Sci. Technol.* **2014**, *4*, 2797−2813.
(62) Lei, Y.; Mehmood, F.; Lee, S.; Greeley, J.; Lee, B.; Seifert, S.; Winans, R. E.; Elam, J. W.; Meyer, R. J.; Redfern, P. C.; Teschner, D.; Schlögl, R.; Pellin, M. J.; Curtiss, L. A.; Vajda, S. *Science* **2010**, *328*, 224−228.
(63) Vajda, S.; Pellin, M. J.; Greeley, J. P.; Marshall, C. L.; Curtiss, L. A.; Ballentine, G. A.; Elam, J. W.; Catillon-Mucherie, S.; Redfern, P. C.; Mehmood, F.; Zapol, P. *Nat. Mater.* **2009**, *8*, 213−216.
(64) Fu, Q.; Saltsburg, H.; Flytzani-Stephanopoulos, M. *Science* **2003**, *301*, 935−938.
(65) Winczewski, S.; Rybicki, J. *Comp. Meth. Sci. Technol.* **2011**, *17*, 75−85.
(66) Sebetci, A. *Chem. Phys.* **2006**, *331*, 9−18.
(67) Bunău, O.; Bartolomé, J.; Bartolomé, F.; Garcia, L. M. *J. Phys.: Condens. Matter* **2014**, *26*, 196006−196017.
(68) Chou, J. P.; Hsing, C. R.; Wei, C. M.; Cheng, C.; Chang, C. M. *J. Phys.: Condens. Matter* **2013**, *25*, 125305−12531.
(69) Moseler, M.; Walter, M.; Yoon, B.; Landman, U.; Habibpour, V.; Harding, C.; Kunz, S.; Heiz, U. *J. Am. Chem. Soc.* **2012**, *134*, 7690−7699.
(70) Hu, C. H.; Chizallet, C.; Mager-Maury, C.; Corral-Valero, M.; Sautet, P.; Toulhoat, H.; Raybaud, P. *J. Catal.* **2010**, *274*, 99−110.
(71) Chan, C. W. A.; Mahadi, A. H.; Li, M. M.; Corbos, E. C.; Tang, C.; Jones, G.; Kuo, W. C. H.; Cookson, J.; Brown, C. M.; Bishop, P. T.; Tsang, S. C. E. *Nat. Commun.* **2014**, *5*, 5787−5795.
(72) Krawczyk, M.; Sobczak, J.; Palczewska, W. *Catal. Lett.* **1993**, *17*, 21−28.

DOI: 10.1021/acscatal.5b01513
ACS Catal. 2015, 5, 5719−5727